Available online at www.sciencedirect.com

ScienceDirect

Journal of Magnesium and Alloys 8 (2020) 910–916

www.elsevier.com/locate/jma

Full Length Article

Fabrication of high-strength duplex nanoporous Cu by dealloying a dual-phase Mg–Cu precursor alloy

Si-Young Lee[a], Soo-Min Baek[a], Eun-Ji Gwak[a], Na-Ri Kang[a], Ju-Young Kim[a], Su-Hyeon Kim[b], Jung Gu Lee[c], Sung Soo Park[a,*]

[a] *School of Materials Science and Engineering, Ulsan National Institute of Science and Technology, Ulsan 44919, Republic of Korea*
[b] *Korea Institute of Materials Science, Changwon 51508, Republic of Korea*
[c] *School of Materials Science and Engineering, University of Ulsan, Ulsan 44610, Republic of Korea*

Received 9 September 2019; received in revised form 19 February 2020; accepted 23 February 2020
Available online 29 May 2020

Abstract

Duplex nanoporous Cu was successfully fabricated by dealloying a dual-phase Mg–Cu precursor alloy consisting of intermetallic Mg_2Cu and $MgCu_2$. The duplex nanoporous Cu with embedded nanoporous struts exhibited highly enhanced strength compared to the typical monolithic nanoporous Cu under both compressive and flexural test conditions at room temperature; the duplex np-Cu sample exhibited a 12 times higher compressive strength and a 40 times greater flexural strength than the monolithic np-Cu sample. Factors responsible for the strength enhancement in the duplex nanoporous Cu are discussed.

Keywords: Mg–Cu alloy; Nanoporous Cu; Dealloying; Duplex structure; Strength.

1. Introduction

Nanoporous materials have recently attracted considerable interest due to their functionality in sensors [1,2], catalysts [3,4], and actuators [5,6]. Furthermore, they show promise for the development of high specific-strength materials [7,8]. Among a variety of fabrication methods reported thus far [9–13], dealloying is considered one of the most efficient ways of producing nanoporous-structured metallic materials. Generally, dealloying is applied to single-phase precursor alloys, which consist of two elements or more with different electrochemical nobility. While an electrochemically less noble element in the precursor material selectively dissolves into an electrolyte during the dealloying process, a relatively nobler element remains undissolved and a nanoporous structure is then formed via atomic diffusion [14].

Despite the advantages of dealloying in fabricating nanoporous structures, nanoporous metals produced via dealloying usually have suffered from issues related to their mechanical properties. Crack formation due to volume shrinkage, frequently occurring during dealloying, has been one of the major factors underlying fragility of dealloyed nanoporous metals, retarding their practical applications [15–17]. Fortunately, it has been recently reported that the presence of shrinkage-induced cracks can be controlled by optimizing the dealloying conditions or compositional modification of a precursor alloy [18–20]. For instance, Sun and Balk showed that nanoporous Au with minimal cracking can be obtained by a multi-step dealloying process [18]. Seker et al. reported that micro-void formation in nanoporous Au films can be reduced by dealloying of precursor Au–Ag films after thermal treatment [19]. Furthermore, Wang et al. found that the inner cracking of nanoporous Cu (np-Cu) can be reduced by microalloying of the Cu–Mn precursor alloy with Si [20].

As indicated above, recent endeavors to improve the mechanical properties of dealloyed nanoporous metals have

* Corresponding author.
E-mail address: sspark@unist.ac.kr (S.S. Park).

https://doi.org/10.1016/j.jma.2020.02.015

been mainly focused on suppressing crack formation during dealloying. However, little attention has been paid to utilizing structural heterogeneity to further improve the mechanical properties of nanoporous metals. In this study, heterogeneously-structured np-Cu having two types of nanoporous constituents was successfully fabricated by dealloying of dual-phase Mg–Cu precursor alloy, and the mechanical properties of the duplex np-Cu were comparatively investigated with those of typical monolithic np-Cu dealloyed from single-phase Mg–Cu precursor alloy.

2. Experimental

Two precursor Mg–Cu alloys with nominal compositions (at%) of Mg–33.3Cu and Mg–36.7Cu were prepared by induction melting using graphite crucibles under an inert atmosphere with a CO_2 and SF_6 mixture and subsequent pouring into a steel mold at ambient temperature. After homogenizing at 450 °C for 24 h and subsequent water quenching, the alloys were cut into a cubic shape with a side length of 3 mm. The alloy samples were ground with SiC papers up to 1200 grit under a water atmosphere; they were then polished using 1 μm diamond paste and 0.04 μm colloidal silica solution under an ethanol atmosphere. Free-corrosion dealloying was conducted in a 1.5 wt% HCl solution at 0 °C to selectively leach Mg atoms from the precursor alloys. Dealloying proceeded until no bubbles appeared to form and the np-Cu samples obtained via dealloying were then subjected to ultrasonic rinsing with ethanol for 1 min.

Microstructural characteristics were investigated using a Hitachi S-4800 scanning electron microscope (SEM), a Quanta 200 field-emission SEM with a TSL electron backscatter diffraction (EBSD) data collection system, and a JEM-2100F Cs-corrected transmission electron microscope (TEM) equipped with an energy dispersive spectrometer. Samples for TEM analysis were prepared using a focused ion beam technique. Three-dimensional (3D) microstructure reconstruction was conducted for the Mg–36.7Cu precursor alloy using a UES Robo-Met.3D automated serial sectioning system. Thermodynamic calculations were conducted using Pandat 2012.

For the evaluation of the mechanical response at a selected area, nanoindentation tests were carried out at room temperature using a Berkovich indenter and continuous stiffness measurement with a Keysight G200. Hardness and elastic modulus values were acquired from nanoindentation at indentation depths of 7∼8 μm according to the method proposed by Oliver and Pharr [21]. The mechanical properties of the np-Cu samples were investigated using compressive and three-point flexural tests at room temperature. The compressive and flexural tests were conducted at an initial strain rate of 3×10^{-3} s^{-1} using cubic compressive specimens with a side length of 3 mm and rectangular flexural specimens with a length of 8 mm, a width of 3 mm, and a thickness of 1.5 mm, respectively.

3. Results and discussion

Fig. 1a and b show SEM micrographs of the Mg–Cu precursor alloys. It can be seen that the Mg–33.3Cu and Mg–36.7Cu alloys have single-phase and dual-phase microstructures, respectively. The EBSD phase analysis results given in Fig. 1c and d indicated that the former has Mg_2Cu phase only and the latter has both Mg_2Cu and $MgCu_2$ phases in their microstructures. This is well consistent with the Mg–Cu binary phase diagram in Fig. 1e. The Mg_2Cu and $MgCu_2$ phases have been known to have an orthorhombic structure with lattice parameters of $a = 0.907$ nm, $b = 0.528$ nm, and $c = 1.825$ nm (ICSD no. 103,047) and a face-centered cubic structure with a lattice parameter of 0.703 nm (ICSD no. 46,007), respectively. The dual-phase microstructure of the Mg–36.7Cu alloy is similar to that of cast Al–Si alloy containing eutectic Si phase [22]. The 3D-reconstructed image in Fig. 1f reveals that the $MgCu_2$ phase in the Mg–36.7Cu alloy is interconnected within the Mg_2Cu matrix. The volume fraction of the $MgCu_2$ phase in the Mg–36.7Cu alloy was measured from the 3D image and found to be ∼9.4%. The two precursor alloys were subjected to the same dealloying procedures for the fabrication of np-Cu. The appearances of the Mg–36.7Cu precursor alloy and np-Cu obtained after dealloying are comparatively shown in Fig. 2. Differences in size and color can be seen between the precursor alloy and dealloyed np-Cu.

Fig. 3a shows a low-magnification SEM micrograph obtained after dealloying of the Mg–33.3Cu alloy. It discloses some macroscopic cracks, which were not present prior to dealloying. As mentioned above, the formation of such inner cracks is generally ascribed to volume shrinkage during dealloying [15]. The high-magnification SEM and TEM micrographs in Fig. 3b–e display np-Cu structures obtained after dealloying. The np-Cu made from the Mg–33.3Cu alloy was found to have a monolithic nanoporous structure with well-linked ligaments with a thickness of 36.0 ± 6.1 nm, analogous to other dealloyed nanoporous metals reported previously [23–25]. The relative density of the monolithic np-Cu was measured and found to be ∼0.27.

On the other hand, the np-Cu prepared from the Mg–36.7Cu alloy presented a duplex nanoporous structure having two different types of np-Cu parts, which appeared to correspond to the Mg_2Cu and $MgCu_2$ phases existing prior to dealloying. This suggests that each np-Cu part constructed via dealloying was strongly affected by the type of pre-existing intermetallic phase in the precursor alloy. Hereafter, the np-Cu parts from the Mg_2Cu and $MgCu_2$ phases are denoted as np-Cu I and np-Cu II, respectively. It should be noted here that the inner cracks observable in the np-Cu I part were not present in the np-Cu II part. In terms of morphology, the duplex np-Cu sample can be characterized by the incorporation of the continuous np-Cu II struts within the np-Cu I matrix. Analysis of the TEM diffraction patterns in Fig. 3f and g confirmed that Cu is the only substance constituting the ligaments of the np-Cu I and np-Cu II parts. The measured ligament thicknesses of the np-Cu I and np-Cu II parts in the duplex np-Cu sample were 34.0 ± 5.7 nm and 21.4 ± 5.5 nm, respec-

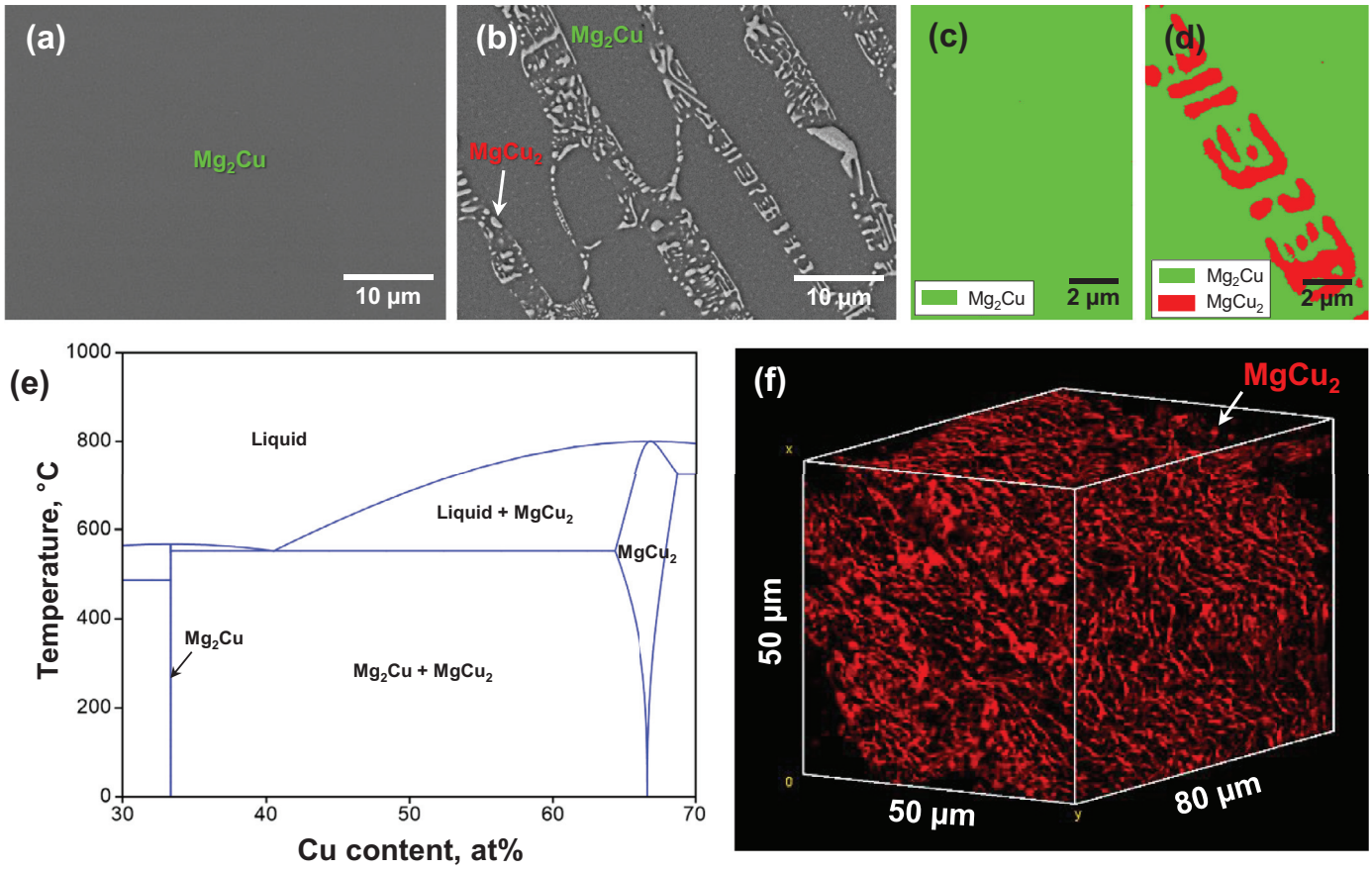

Fig. 1. SEM micrographs of the (a) Mg–33.3Cu and (b) Mg–36.7Cu precursor alloys, EBSD phase maps of the (c) Mg–33.3Cu and (d) Mg–36.7Cu precursor alloys, (e) a Mg–Cu binary phase diagram, and (f) a 3D-reconstructed image of the Mg–36.7Cu precursor alloy.

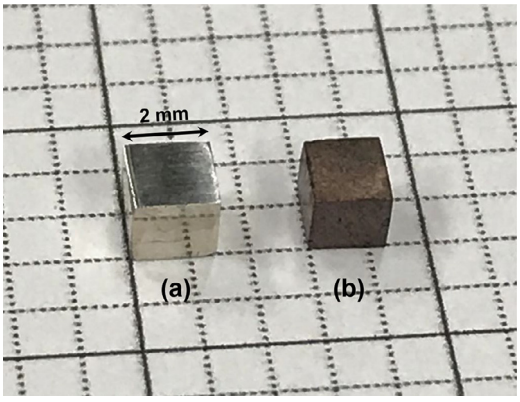

Fig. 2. Appearances of the cuboidal samples (a) before and (b) after dealloying the Mg–36.7Cu precursor alloy.

tively. Although the relative density of the embedded np-Cu II part cannot be directly measured, it is expected to be much larger than that of the np-Cu I part, considering the Cu to Mg atomic ratios of the corresponding intermetallic phases. The monolithic and duplex np-Cu samples are schematically represented in Fig. 4.

Nanoindentation tests were carried out to separately investigate the mechanical response of each nanoporous part in the duplex np-Cu sample. Fig. 5 shows the force-indentation depth curves of the np-Cu I and np-Cu II parts and corresponding hardness and elastic modulus variations of the np-Cu I and np-Cu II parts as a function of indentation depth are given in Fig. 6. As listed in Table 1, hardness values were found to be 25.4 ± 0.6 and 70.4 ± 0.5 MPa for the np-Cu I and np-Cu II parts, respectively, showing that the np-Cu II part has a ~3 times greater hardness value than the np-Cu I part. Furthermore, elastic modulus values were found to be 206.9 ± 6.9 and 2858.1 ± 95.8 MPa for the np-Cu I and np-Cu II parts, respectively, indicating that the difference in elastic modulus (~14 times) is much larger than that in hardness between the np-Cu I and np-Cu II parts. These nanoindentation results suggest that the duplex np-Cu sample additionally having the np-Cu II part would provide advantages in strength-related properties over the monolithic np-Cu sample without it.

Table 1
Hardness and elastic modulus values obtained from the nanoindentation tests for the np-Cu I and np-Cu II parts of the duplex np-Cu sample.

Type	Hardness (MPa)	Elastic modulus (MPa)
np-Cu I	25.4 ± 0.6	206.9 ± 6.9
np-Cu II	70.4 ± 0.5	2858.1 ± 95.8

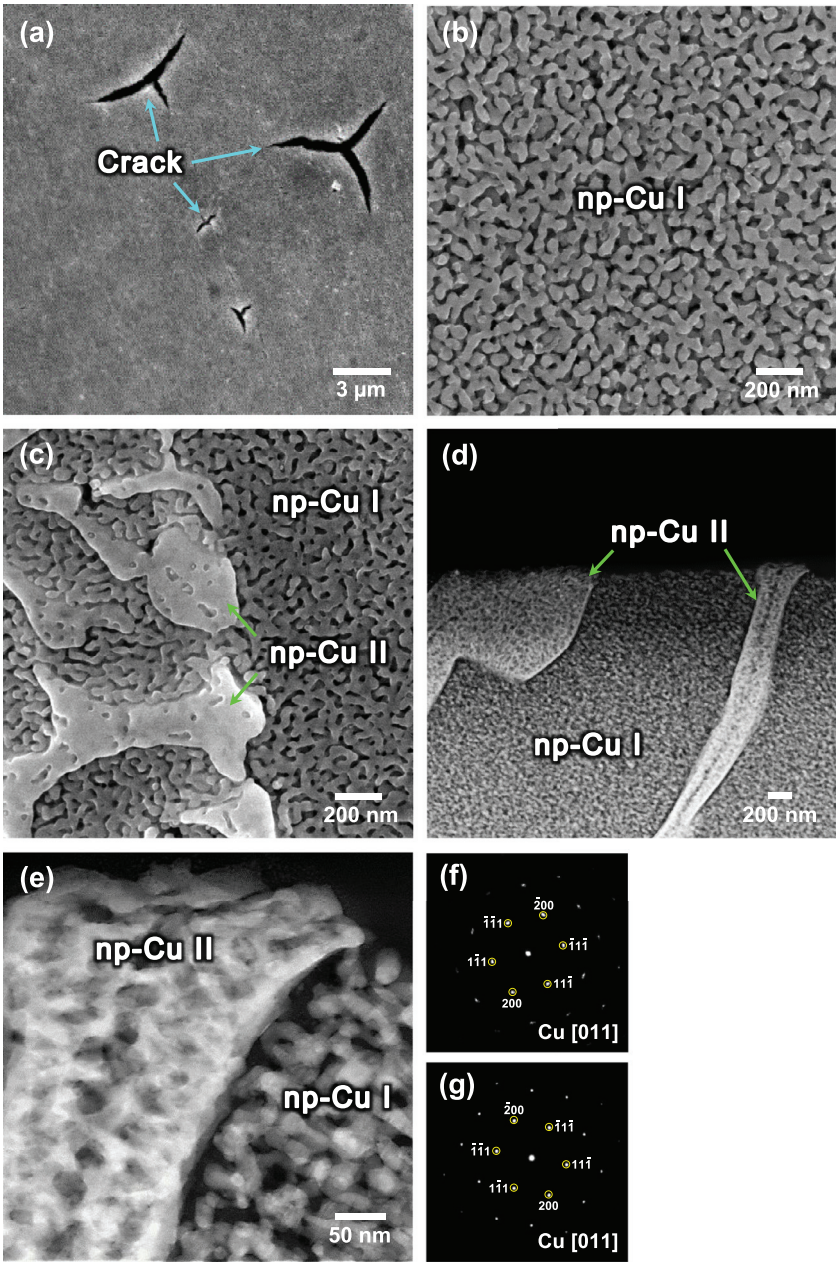

Fig. 3. (a) Low-magnification and (b) high-magnification SEM micrographs of the monolithic np-Cu sample and high-magnification (c) SEM and (d,e) TEM micrographs of the duplex np-Cu sample with the diffraction patterns obtained from the (f) np-Cu I and (g) np-Cu II parts in the TEM micrograph.

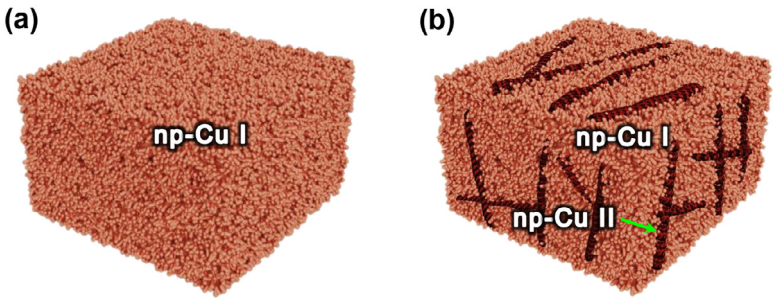

Fig. 4. Schematic diagrams of the (a) monolithic and (b) duplex np-Cu samples.

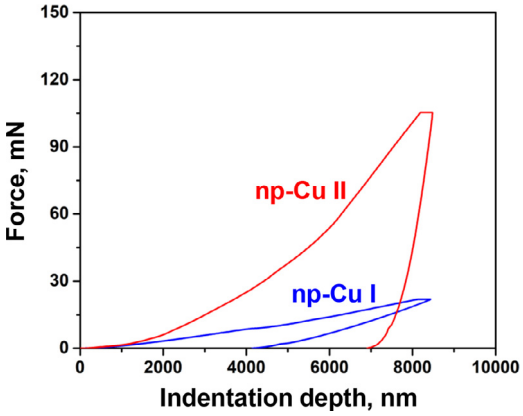

Fig. 5. Force-indentation depth curves of the np-Cu I and np-Cu II parts in the duplex np-Cu sample.

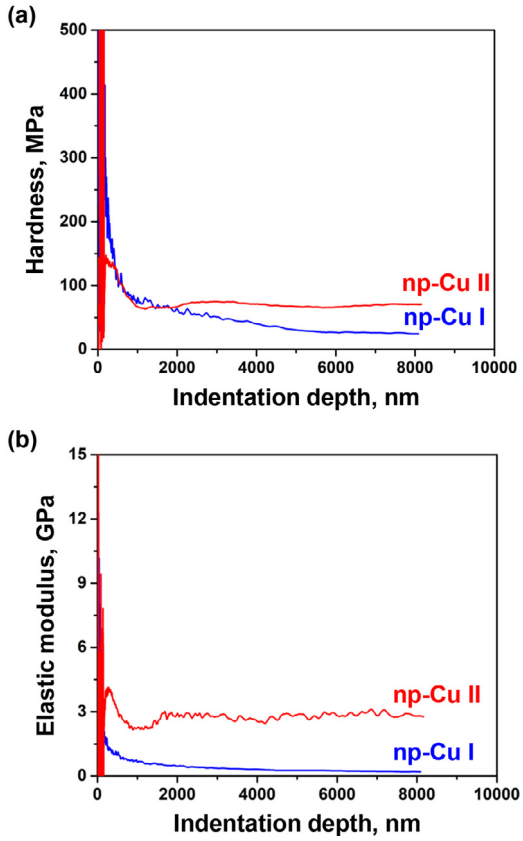

Fig. 6. Variations in (a) hardness and (b) elastic modulus of the np-Cu I and np-Cu II parts in the duplex np-Cu sample as a function of indentation depth.

Fig. 7a provides the compressive stress-strain curves of the monolithic and duplex np-Cu samples. The monolithic np-Cu sample showed a low compressive yield strength of 1.3 ± 0.6 MPa at the early stage of compressive strain. This was followed by a stress plateau and a densification-induced stress increase, phenomena that are typically observed during the compressive deformation of nanoporous materials [26,27]. On the other hand, the duplex np-Cu sample showed a steeper slope in the elastic region and a higher yield point as compared to the monolithic np-Cu sample. It displayed a compressive yield strength (CYS) of 15.4 ± 1.5 MPa, which is ~12 times greater than the CYS of the monolithic np-Cu sample. The plateau region observed in the monolithic np-Cu sample did not appear in the duplex np-Cu sample. Instead, stress was found to considerably drop after a yield point, which was followed by a rather gradual stress increase at strains exceeding ~35% due to densification. Such a stress drop after yielding has been similarly shown in np-Cu fabricated by dealloying of Al–Cu precursor alloys [28].

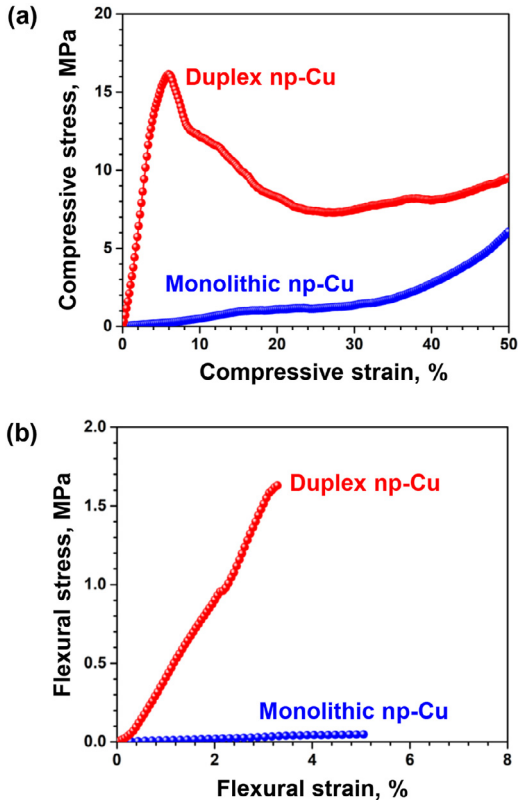

Fig. 7. (a) Compressive and (b) flexural stress-strain curves of the monolithic and duplex np-Cu samples.

Furthermore, the flexural stress-strain curves of the monolithic and duplex np-Cu samples are provided in Fig. 7b. Although the overall stress levels of the curves were quite low, the difference in strength between the np-Cu samples was found to be more pronounced in the flexural test results than in the compressive test results. The monolithic and duplex np-Cu samples exhibited maximum flexural strengths of 0.04 ± 0.03 and 1.7 ± 0.2 MPa, respectively, indicating that the latter is ~40 times stronger than the former under the flexural test conditions.

The strength of nanoporous materials has been interpreted using scaling equations having structure-related variables such as relative density and ligament size [16,29–31]. A calculation using the Hodge equation [30], $\sigma_y = 0.3(\sigma_s + \frac{k}{\sqrt{t}})\rho_r^{1.5}$, where σ_y is the yield strength of nanoporous metal, σ_s is the yield strength of bulk metal (σ_s=33~333.4 MPa for Cu) [32], k is a strength coefficient (k=0.14 MPa $m^{0.5}$ for Cu)

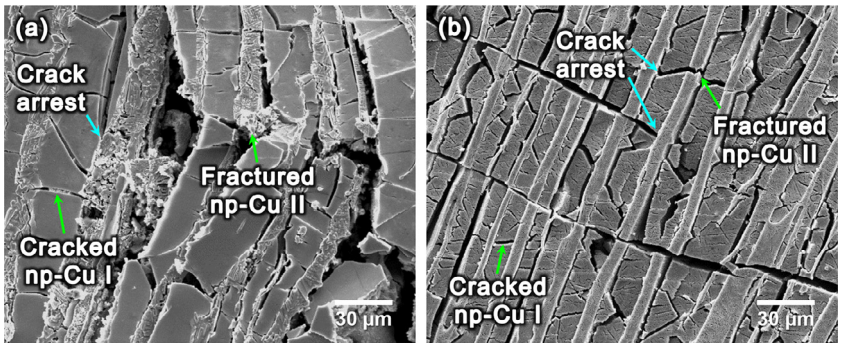

Fig. 8. SEM micrographs of the duplex np-Cu samples (a) after a compressive strain of 0.06 and (b) after a flexural strain of 0.03.

[33], t is the ligament thickness (t=36 nm in this study), and ρ_r is the relative density (ρ_r=0.27 in this study), indicated that the expected yield strength of the monolithic np-Cu sample is in a range of 32.4∼45.1 MPa. A calculation using the scaling law recently proposed by Huber et al. [31], $\sigma_y = c \cdot \sigma_{yS}(\frac{r}{l})^3(1-\sqrt{6}\ c_R\frac{r}{l})^{-1}$, where c is a coefficient of ∼1.4 [31], σ_{yS} is the yield strength of a ligament, r is the ligament radius (r=18 nm in this study), l is the spacing between nodes connecting ligaments (l=∼50 nm in this study), and c_R is a geometry parameter of ∼1.1 [31], also indicated that the yield strength of the monolithic np-Cu sample should be higher than 6.5 MPa, considering that σ_{yS} is greater than σ_s [34–36]. Besides these calculations, the hardness value of the monolithic np-Cu sample (25.4 MPa) corresponds to yield strengths of 8.5∼9.6 MPa, according to recent reports on relationship between the hardness and yield strength of nanoporous materials [27,37,38]. However, the sample was experimentally shown to have a compressive yield strength of only ∼1.3 MPa, suggesting the occurrence of premature fracture during the compressive test. In this regard, the discrepancy between the predicted and experimental strength values can be attributed to a detrimental effect of dealloying-induced inner cracks on maintaining high strength.

On the other hand, the duplex np-Cu sample has much higher levels of strength under both compressive and flexural test conditions than the monolithic np-Cu sample. Since nearly no difference was detected between the np-Cu I parts of the monolithic and duplex np-Cu samples, the relatively enhanced strength observed in the latter can be considered closely associated with its incorporation of the np-Cu II part. As indicated in Fig. 8, observations of the duplex np-Cu samples subjected to compressive and flexural stress conditions clearly revealed that the np-Cu II part acted as supporting struts or frames, which can resist dimensional change under an applied stress and also can prevent the propagation of cracks formed in the np-Cu I part. These roles of the np-Cu II part in load-bearing and crack-arresting are consistent with the aforementioned nanoindentation results, showing that the np-Cu II part has higher levels of hardness and elastic modulus than the np-Cu I part. This beneficial influence of the supporting np-Cu II struts on strengthening would be more effective when combined with an improvement in the structural integrity of the np-Cu I matrix.

4. Conclusion

Dual-phase and single-phase Mg–Cu precursor alloys were subjected to free-corrosion dealloying for the fabrication of duplex and monolithic np-Cu samples, respectively. The duplex np-Cu sample having both np-Cu I and np-Cu II parts exhibited a 12 times higher compressive strength and a 40 times greater flexural strength than the monolithic np-Cu sample without the np-Cu II part. The compressive and flexural strengthening observed in the duplex np-Cu sample was attributed to the load-bearing and crack-arresting effects of the embedded np-Cu II part, which acted as supporting struts.

Acknowledgment

This work was supported by the National Research Foundation of Korea (NRF) grant funded by the Korea government (MSIT) (No. 2019R1A2C1003905).

References

[1] K. Hotta, A. Yamaguchi, N. Teramae, Nanoporous waveguide sensor with optimized nanoarchitectures for highly sensitive label-free biosensing, ACS Nano 6 (2012) 1541–1547.
[2] R. Song, Zhang L, F. Zhu, W. Li, Z. Fu, B. Chen, M. Chen, H. Zeng, D. Pan, Hierarchical nanoporous copper fabricated by one-step dealloying toward ultrasensitive surface-enhanced Raman sensing, Adv. Mater. Interfaces 5 (2018) 1800332.
[3] M. Yan, T. Jin, Y. Ishikawa, T. Minato, T. Fujita, L.-.Y. Chen, M. Bao, N. Asao, M.-.W. Chen, Y. Yamamoto, Nanoporous gold catalyst for highly selective semihydrogenation of alkynes: remarkable effect of amine additives, J. Am. Chem. Soc. 134 (2012) 17536–17542.
[4] T.T.H. Hoang, S. Verma, S. Ma, T.T. Fister, J. Timoshenko, A.I. Frenkel, P.J.A. Kenis, A.A. Gewirth, Nanoporous copper–silver alloys by additive-controlled electrodeposition for the selective electroreduction of CO_2 to ethylene and ethanol, J. Am. Chem. Soc. 140 (2018) 5791–5797.
[5] D. Kramer, R.N. Viswanath, J. Weissmüller, Surface-stress induced macroscopic bending of nanoporous gold cantilevers, Nano Lett. 4 (2004) 793–796.
[6] J. Zhang, L. Lv, H. Gao, Q. Bai, C. Zhang, Z. Zhang, Electrochemical actuation behaviors and mechanisms of bulk nanoporous Ni–Pd alloy, Scr. Mater. 137 (2017) 73–77.
[7] J. Biener, A.M. Hodge, A.V. Hamza, L.M. Hsiung, J.H. Satcher Jr., Nanoporous Au: a high yield strength material, J. Appl. Phys. 97 (2005) 024301.
[8] H. Kashani, Y. Ito, J. Han, P. Liu, M. Chen, Extraordinary tensile strength and ductility of scalable nanoporous graphene, Sci. Adv. 5 (2019) eaat6951.

[9] J. Erlebacher, M.J. Aziz, A. Karma, N. Dimitrov, K. Sieradzki, Evolution of nanoporosity in dealloying, Nature 410 (2001) 450–453.
[10] J. Yu, Y. Ding, C. Xu, A. Inoue, T. Sakurai, M. Chen, Nanoporous metals by dealloying multicomponent metallic glasses, Chem. Mater. 20 (2008) 4548–4550.
[11] C. Li, M. Iqbal, J. Lin, X. Luo, B. Jiang, V. Malgras, K.C.-W. Wu, J. Kim, Y. Yamauchi, Electrochemical deposition: an advanced approach for templated synthesis of nanoporous metal architectures, Acc. Chem. Res. 51 (2018) 1764–1773.
[12] M. Mao, Y. Tang, K. Zhao, Z. Duan, C. Wu, Porous titanium scaffolds with aligned lamellar pore channels by directional freeze-casting from aqueous TiH_2 slurries, Met. Mater. Int. 25 (2019) 508–515.
[13] Y.-J. Yi, M.-J. Lee, J.-Y. Yun, B.-K. Kim, Fabrication of a porous Ni-based metal with a multi-pore structure by a screen printing process, Met. Mater. Int. 25 (2019) 1272–1277.
[14] L.H. Qian, M.W. Chen, Ultrafine nanoporous gold by low-temperature dealloying and kinetics of nanoporous formation, Appl. Phys. Lett. 91 (2007) 083105.
[15] S. Parida, D. Kramer, C.A. Volkert, H. Rösner, J. Erlebacher, J. Weissmüller, Volume change during the formation of nanoporous gold by dealloying, Phys. Rev. Lett. 97 (2006) 035504.
[16] E.-J. Gwak, J.-Y. Kim, Weakened flexural strength of nanocrystalline nanoporous gold by grain refinement, Nano Lett. 16 (2016) 2497–2502.
[17] H. Kashani, M. Chen, Flaw-free nanoporous Ni for tensile properties, Acta Mater. 166 (2019) 402–412.
[18] Y. Sun, T.J. Balk, A multi-step dealloying method to produce nanoporous gold with no volume change and minimal cracking, Scr. Mater. 58 (2008) 727–730.
[19] E. Seker, M.L. Reed, M.R. Begley, A thermal treatment approach to reduce microscale void formation in blanket nanoporous gold films, Scr. Mater. 60 (2009) 435–438.
[20] Y.M. Wang, W. Zhang, A. Inoue, Nanoporous Cu wide ribbons with good mechanical integrity, Mater. Sci. Eng. B 177 (2012) 532–535.
[21] W.C. Oliver, G.M. Pharr, An improved technique for determining hardness and elastic modulus using load and displacement sensing indentation experiments, J. Mater. Res. 7 (1992) 1564–1583.
[22] S. Hegde, K.N. Prabhu, Modification of eutectic silicon in Al–Si alloys, J. Mater. Sci. 43 (2008) 3009–3027.
[23] J. Erlebacher, An atomistic description of dealloying, J. Electrochem. Soc. 151 (2004) C614–C616.
[24] J.R. Hayes, A.M. Hodge, J. Biener, A.V. Hamza, Monolithic nanoporous copper by dealloying Mn–Cu, J. Mater. Res. 21 (2006) 2611–2616.
[25] H.-B. Lu, Y. Li, F.-H. Wang, Synthesis of porous copper from nanocrystalline two-phase Cu–Zr film by dealloying, Scr. Mater. 56 (2007) 165–168.
[26] N. Mameka, K. Wang, J. Markmann, E.T. Lilleodden, J. Weissmüller, Nanoporous gold–testing macro-scale samples to probe small-scale mechanical behavior, Mater. Res. Lett 4 (2016) 27–36.
[27] H.-J. Jin, L. Kuramanaeva, J. Schmauch, H. Rösner, Y. Ivanisenko, J. Weissmüller, Deforming nanoporous metal: role of lattice coherency, Acta Mater. 57 (2009) 2665–2672.
[28] F. Chen, X. Chen, L. Zou, Y. Yao, Y. Lin, Q. Shen, E.J. Lavernia, L. Zhang, Fabrication and mechanical behavior of bulk nanoporous Cu via chemical de-alloying of Cu–Al alloys, Mater. Sci. Eng. A 660 (2016) 241–250.
[29] L.J. Gibson, M.F. Ashby, Cellular Solids: Structure and Properties, Second Ed., Cambridge University Press, Cambridge, 2001.
[30] A.M. Hodge, J. Biener, J.R. Hayes, P.M. Bythrow, C.A. Volkert, A.V. Hamza, Scaling equation for yield strength of nanoporous open–cell foams, Acta Mater. 55 (2007) 1343–1349.
[31] N. Huber, R.N. Viswanath, N. Mameka, J. Markmann, J. Weissmüller, Scaling laws of nanoporous metals under uniaxial compression, Acta Mater. 67 (2014) 252–265.
[32] J.R. Davis, ASM Specialty Handbook: Copper and Copper Alloys, ASM International, Ohio, 2001.
[33] N. Hansen, Hall-Petch relation and boundary strengthening, Scr. Mater. 51 (2004) 801–806.
[34] D. Kiener, W. Grosinger, G. Dehm, R. Pippan, A further step towards an understanding of size-dependent crystal plasticity: in situ tension experiments of miniaturized single-crystal copper samples, Acta Mater. 56 (2008) 580–592.
[35] A.T. Jennings, M.J. Burek, J.R. Greer, Microstructure versus size: mechanical properties of electroplated single crystalline Cu nanopillars, Phys. Rev. Lett. 104 (2010) 135503.
[36] A.T. Jennings, J.R. Greer, Tensile deformation of electroplated copper nanopillars, Philos. Mag. 91 (2011) 1108–1120.
[37] N.J. Briot, T.J. Balk, Developing scaling relations for the yield strength of nanoporous gold, Philos. Mag. 95 (2015) 2955–2973.
[38] Y.-C. Kim, E.-J. Gwak, S.-M. Ahn, J.-I. Jang, H.N. Han, J.-Y. Kim, Indentation size effect in nanoporous gold, Acta Mater. 138 (2017) 52–60.